



# Warm bias of sea surface temperature in Eastern boundary current regions—a study of effects of horizontal resolution in CESM

Jialiang Ma<sup>1</sup> · Shiming Xu<sup>1</sup> · Bin Wang<sup>1</sup>

Received: 25 December 2018 / Accepted: 4 June 2019 / Published online: 9 July 2019  
© Springer-Verlag GmbH Germany, part of Springer Nature 2019

## Abstract

Warm bias of modeled sea surface temperature (SST) in the eastern boundary upwelling systems (EBUS) is a ubiquitous feature in coupled climate models. This paper investigates the causes underlying this warm bias, with a focus on the effect of horizontal resolution in the atmospheric component of coupled models, by using Community Earth System Model (CESM) as an example. By breaking down the energy budget of the upper ocean, we conclude that surface net heat flux and Ekman upwelling process exert a considerable influence (over 80%) on upper ocean temperature of EBUS in CESM. Besides, the problem of underestimation of stratocumulus cloud is not present near the coast, and hence not responsible for this warm bias in CESM. On the contrary, downward shortwave radiation bias is overcompensated by longwave radiation and latent flux bias on the open ocean. Therefore, the insufficient ocean dynamic upwelling is the dominantly cause for SST warm bias. Finer horizontal resolution atmosphere component of CESM enables better representation of low-level coastal jet structure, with stronger and closer alongshore wind stress and curl leading to realistic representation of upwelling process and horizontal water mass transportation. Furthermore, low-level coastal jet is shown to be sensitive to coastal mountain topography, especially in South East Pacific region, through both thermodynamic and dynamic atmospheric processes and oceanic response. This article provides further proof of improving coupled climate models in reducing the SST biases in EBUS regions.

**Keywords** Sea-surface temperature · Coastal upwelling · Wind stress · Topography

## 1 Introduction

Eastern boundary upwelling systems (EBUS) are located in the eastern boundaries of the tropical and subtropical oceans, and they are regions of mass exchange between

surface and inner ocean and high biological productivity. As a result of the land-sea distribution, the regions are usually characterized by strong upwelling driven by along-shore prevailing wind. The cold nutrient-rich deep water is upwelled toward the ocean surface, leading to the cooling of sea surface temperature (SST). However, climate models often have trouble in realistic representation of these regions. For example, most Coupled Model Intercomparison Project Phase 5 (CMIP5) models show substantial SST warm biases in EBUS (Wang et al. 2014; Richter 2015), especially in southeast tropical Atlantic region. The biases undermine the ability of climate models in climate projections, as well as the representation of biogeochemical processes and their potential changes in the future.

Many previous studies have been investigating the sources of warm biases in typical southeast Pacific and Atlantic regions. From the atmosphere perspective, excessive shortwave radiation caused by underestimation of stratocumulus decks is a key reason (Huang et al. 2007). Furthermore, the increased SST due to the excessive shortwave radiation could result in decreasing the lower

---

This article is part of the Topical Collection on the *10th International Workshop on Modeling the Ocean (IWMO), Santos, Brazil, 25–28 June 2018*

---

Responsible Editor: Tal Ezer

---

✉ Shiming Xu  
xusm@tsinghua.edu.cn

Jialiang Ma  
mj114@mails.tsinghua.edu.cn

Bin Wang  
wab@tsinghua.edu.cn

<sup>1</sup> Department of Earth System Science, Tsinghua University, 100084 Beijing, China

tropospheric stability, which further inhibits the oceanic low cloud formation and existence. This so-called cloud-SST positive feedback probably contributes to the SST warm bias in large open-ocean regions (Hu et al. 2008; Ma et al. 1996). However, some studies show contradictory results: Large and Danabasoglu (2006) argued that the solar radiation bias in Community Climate System Model version 3 (CCSM3) is unable to raise SST by more than about 1° and coastal upwelling errors may have more contribution to the SST bias. Similarly, Xu et al. (2014) showed that the shortwave radiation error was overcome by larger errors in the simulated surface turbulent heat and longwave radiation fluxes, resulting in excessive heat loss from the ocean.

Meanwhile, coastal upwelling is strongly sensitive to the structure and strength of alongshore wind of the subtropical anticyclones. Climate models are commonly characterized by weaker low-level alongshore wind when compared with observations, leading to insufficient upwelling (Large and Danabasoglu 2006; Xu et al. 2014; Wahl et al. 2011). Richter (2015) summarized that both the maximum wind speed and the maximum wind stress curl were displaced offshore in GCMs, often by hundreds of kilometers. The low-level coastal jet is always controlled by large-scale subtropical anticyclone, land-sea thermal contrast, and steep coastal topography. Holt (1996) suggested the effect of coastal topography was to act as a barrier to the onshore intrusion of higher momentum offshore air. Jung et al. (2014) artificially lowered the African topography in CCSM3 and found that uplift of Africa induced intensification of coastal low-level winds, which leads to increased oceanic upwelling.

On the ocean side, the insufficient upwelling in climate models is the major reason for warm SST bias. Wahl et al. (2011) presented the underestimation of upwelling was probably owing to the low resolution of ocean model. Also, the ocean components of the climate models usually have very coarse resolution to resolve eddies, which are capable of transporting cold water from the coast toward the ocean's interior (Colas et al. 2012). However, Zheng et al. (2012) showed the transport process did not significantly impact the heat budget in the southeast Pacific (SEP) ocean by using an eddy-resolving model (1/12°). In addition, Breugem et al. (2010) attributed the warm SST bias to the existence of an erroneous barrier layer (BL) in the east and southeast tropical Atlantic in coupled models. They also pointed out so-called SST-precipitation-BL feedback amplified the warm bias through the prevention of surface cooling, while some other studies suggested the feedback played a less significant role in Atlantic SST warm bias (Richter et al. 2011; Patricola et al. 2012). This is in direct link to the fact that southeast tropical Atlantic features more complicated currents system than Pacific side. The equatorward Benguela current and poleward Angola current

meet between 15 and 17°S, forming the Angola-Benguela Front (ABF) (Mohrholz et al. 2001; Shannon et al. 1987). In Xu et al. (2014), it is emphasized that the failure of simulating the ABF position was a major source of the warm SST bias.

With the gradual increase of model resolutions in climate studies, there exists potential in improving the modeling of EBUS regions with higher resolution of the atmospheric components. Gent et al. (2010) illustrated that the strongest surface winds in the upwelling regions located much nearer the coasts when comparing 0.5° atmosphere resolution with 2° in CCSM. As a result, the warm bias magnitude was to some extent reduced with finer atmosphere resolution, especially in southeast Pacific side. Meanwhile, Small et al. (2015) carried out a series of sensitivity experiments with different atmosphere and ocean resolution, respectively. It is suggested that higher atmosphere resolution, up to 0.5°, produced narrower negative wind stress curl alongshore, leading to less poleward water transport dominated by Sverdrup balance. Both theories highlighted the importance of atmosphere resolution in coupled climate models. Therefore, to assess the attribution of SST warm bias of EBUS in Community Earth System Model (CESM) and the effect of resolution, this paper performed sensitivity experiments involving the horizontal resolution of the atmospheric component.

The paper is organized as follows. Section 2 introduces the model and the numerical experiments, the datasets are used for comparison, as well as the analysis method. Section 3 carries out the analysis of heat budget, and causes of warm SST bias by comparing results between high-resolution and low-resolution settings in CESM. Furthermore, the study of model topography is carried out in Section 4 to further elucidate the effect of resolution and the model's topographic features in SST biases. Finally Section 5 summarizes the article and proposes suggestion for climate model development for the reduction of SST biases in EBUS regions.

## 2 Model and data

### 2.1 Model and numerical experiments

In this study, we adopt the coupled model CESM (version 1) (Hurrell et al. 2013). CESM is a fully coupled, global climate model that could simulate the Earth's climate state. The model contains coupled components, including the Community Atmosphere Model version 4 (CAM4) (Neale et al. 2013), Parallel Ocean Program version 2 (POP2) (Danabasoglu et al. 2012), Community Land Model version 4 (CLM4) (Oleson et al. 2015), and Community Ice Code version 4 (CICE4) (Hunke and Lipscomb 2008). In this

**Table 1** List of experiments

Experiment name	Atmosphere resolution	Ocean resolution	Experiment description
F09	0.9° × 1.25°	~ 1°	Pre-industrial control run, initializes from steady state, integrates for 50 years.
F05	0.47° × 0.63°	~ 1°	Pre-industrial control run, initializes from steady state, integrates for 50 years.
F09_mod	0.9° × 1.25°	~ 1°	Same run as F09, except land topography is replaced by that of F05 in the red rectangle regions of Fig. 1.
F05_mod	0.47° × 0.63°	~ 1°	Same run as F05, except land topography is replaced by that of F09 in the red rectangle regions of Fig. 1.

article, we use the finite volume (FV) dynamical core in CAM4. The two horizontal resolution settings in CAM4 are 0.9° × 1.25° and 0.47° × 0.63°, and they are accompanied with the same 26 vertical levels. POP2 and CICE4 have a nominal 1° horizontal grid spacing with 60 vertical levels.

Table 1 shows the experiments that are carried out with CESM for comparison and analysis. All the experiments are forced with the Pre-Industrial Control run (piControl) from the Climate Model Intercomparison Project Phase 5 (CMIP5) long-term experiments (Taylor et al. 2012). Specifically, the climate forcings of piControl run, such as greenhouse gases, aerosol, ozone, and solar constant, are fixed at the level of year 1850. In this study, we initialize from a steady state, then integrate the model for 50 years. After the spin-up of the models, the results of the last 30 years are used for analysis. First two experiments (F09 and F05) are carried out with different atmosphere horizontal resolution 0.9° × 1.25° and 0.47° × 0.63°. In addition, F09\_mod and F05\_mod experiments aim to study the influence of model’s topography. F09\_mod (F05\_mod) set is the same with F09 (F05), except land topography is replaced by that of F05 (F09) in the red rectangle regions of Fig. 1.

**2.2 Data and method**

SST dataset adopted in this study for comparison with climatology is based on Hurrell et al.’s. SST dataset (Hurrell et al. 2008) during 1870–1900 on 1° grid. It merges monthly mean Hadley Centre sea ice and SST dataset version 1 (HadISST1) and the National Oceanic and Atmospheric Administration (NOAA) weekly optimum interpolation SST version 2 (OISST V2). The consistent, multi-decade, global analysis of shortwave, longwave radiation, sensible and latent heat flux are provided by monthly mean Objectively Analyzed air-sea Flux (OAFlux) (Yu et al. 2012) during 1984–2009 on 1° grid. All of the

4 OAFlux data sets except shortwave are positive upward. The modeled stratocumulus cloud fraction is compared to July 2006–December 2010 CloudSat observations, which is an experimental radar satellite for clouds and precipitation (Stephens et al. 2002). Wind stress, 10m wind velocity, ocean current, and ocean temperature are from the National Centers for Environmental Prediction (NCEP) Climate Forecast System Reanalysis (CFSR) monthly data (Saha et al. 2012) during 1979–2008. The NCEP/CFSR data is based on a global high-resolution coupled ocean-atmosphere system with coupled data assimilation. The horizontal resolution of the CFSR atmospheric component is ~ 0.312°. And CFSR ocean analysis data has horizontal resolution 0.5° with 40 vertical levels. Besides, wind data from long time series mean Common Ocean Reference Experiment version 2 (COREv2) (Large and Yeager 2009) during 1977–2005 on 1° grid is also adopted for comparison. This monthly product is usually used for the forcing of ocean models for inter-comparison. Climatology is averaged during each time period of datasets for comparison in this article.

To assess the contribution of each physical process to surface sea temperature, the time-mean ocean heat balance integrated over the upper ocean based on the heat budget equation (Menkes et al. 2006) is computed as:

$$\frac{\partial \langle T \rangle}{\partial t} = \underbrace{\frac{Q_n}{\rho C_p h}}_A + \underbrace{\left\langle -\bar{u} \frac{\partial \bar{T}}{\partial x} \right\rangle}_B + \underbrace{\left\langle -\bar{v} \frac{\partial \bar{T}}{\partial y} \right\rangle}_C + \underbrace{\frac{1}{h} w_{(z=-h)} (\langle T \rangle - \bar{T}_{(z=-h)})}_D + \underbrace{R}_E \tag{1}$$

where  $Q_n$  is surface net heat flux,  $\rho$  the sea water constant density (1026kg/m<sup>3</sup>),  $C_p$  the constant specific

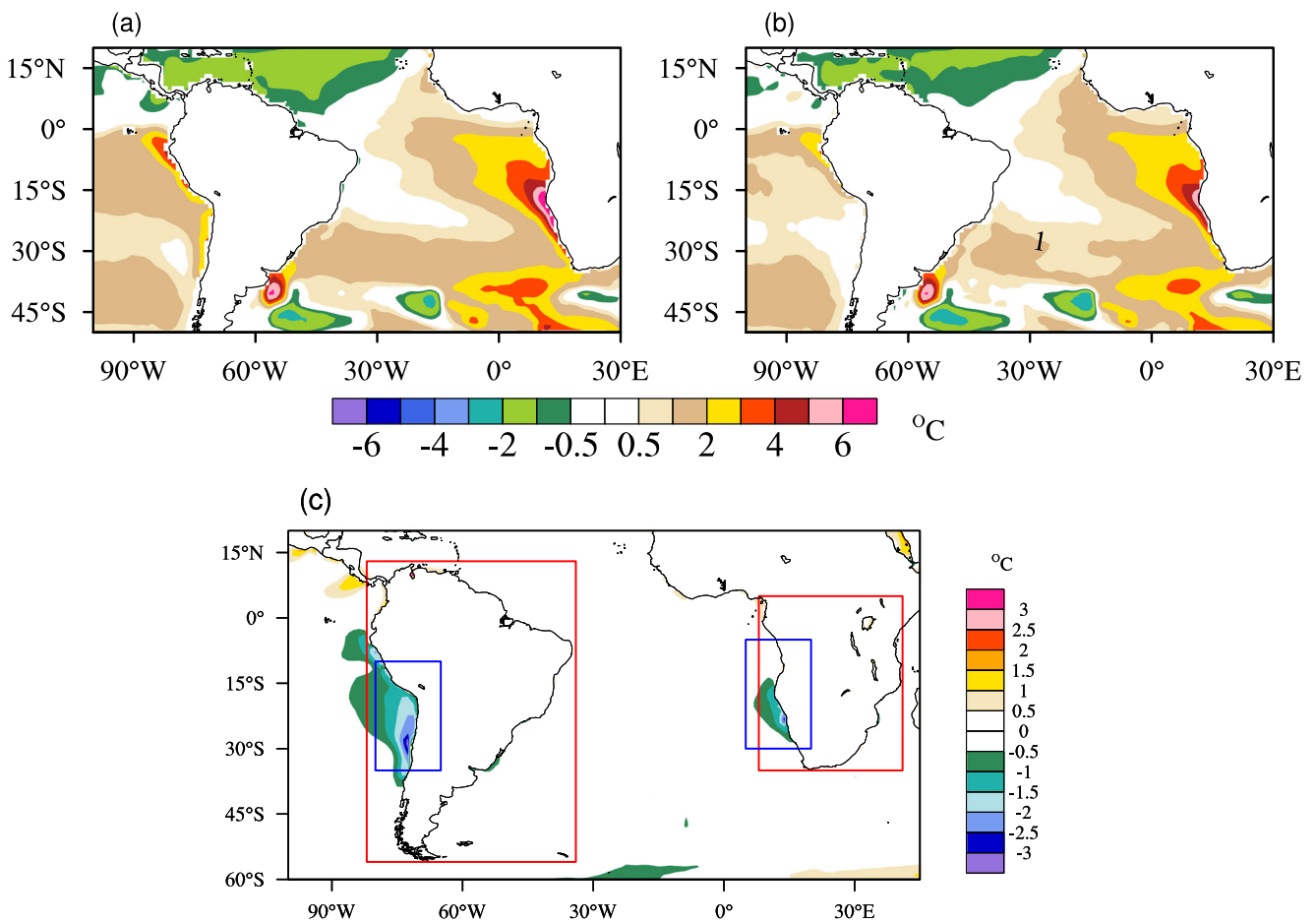


**Fig. 1** Sea Surface Temperature (SST) bias in CESM: **a** for F09, and **b** for F05; **c** the difference between F05 and F09, i.e., (b) minus (a). Blue rectangles are SEP and SEA regions for flux averaging and heat

balance analysis in Section 3.1 and red rectangles mark the regions where land topography is replaced in case F09\_mod and F05\_mod

heat capacity ( $3996J/(kg \cdot K)$ ), and  $h$  the ocean mixed-layer depth.  $u$  and  $v$  are the horizontal ocean current velocities,  $w$  the vertical velocity, and  $T$  the potential temperature. The overbar indicates monthly mean for each variable, while  $\langle \bullet \rangle$  indicate vertical average through the whole mixed layer  $h$ :

$$\langle \bullet \rangle = \frac{1}{h} \int_{-h}^0 \bullet dz \tag{2}$$

Therefore, the left side of Eq. 1 represents temperature tendency, which is governed by all the terms on the right-hand side of the equation. In this article, we calculate this term using climatology mean data from F09 and F05 experiments, respectively, so the result is equal to 0 (i.e., equilibrium). Term A represents net surface heat flux absorbed by ocean. Term B and C are zonal and meridional heat advection, respectively. Term D represents vertical entrainment at the bottom of the mixed layer. E is the residual term from horizontal and vertical diffusion, turbulent mixing and unresolved high-frequency variability

due to averaging during the climatological analysis. The relative contribution of each term is calculated as follows:

$$Con = \frac{|X|}{|A| + |B| + |C| + |D| + |E|} \times 100\% \tag{3}$$

Here, X is one of term A, B, C, D and E in Eq. 1, and  $|\bullet|$  represents absolute value of each term.

### 3 Sources of SST warm bias in CMIP5

In the article, the causes of SST warm bias will be broken down by studying Southeast Pacific (SEP) and Southeast Atlantic (SEA) regions in Southern Hemisphere. For CESM, large warm bias exists in these both upwelling regions and the westward extension areas. Especially, the maximum warm bias is up to over  $6^\circ$  along shore (i.e., the upwelling region) of SEA, while in SEP  $2 \sim 3^\circ$  (Fig. 1a). The effect of atmosphere horizontal resolution is shown in Fig. 1b and c. For higher atmosphere resolution case F05, bias near Peru-Chile coast is reduced at most (by  $2 \sim 3^\circ C$ ).

### 3.1 Heat budget analysis

To assess the contribution to surface ocean temperature, we calculate each term of Eq. 1 for SEA and SEP regions based on the modeled climatology. Figure 2 illustrates the SEA and SEP area averaged contribution of each term for F09 and F05. Among all the terms, surface net heat flux (shortwave minus the sum of longwave, latent flux, and sensible flux) absorbed by upper ocean and vertical entrainment plays an important role in dominating heat budget. Surface net heat flux warms the surface water, while vertical water upwelling cools the ocean, and the sum of two factors contributes to over 80% of the SST changes in all experiments. However, surface net heat flux contributes more than vertical upwelling process in SEA, while for SEP the effect is opposite. The result demonstrates the difference in the dominant processes in SEA and SEP region. Meanwhile, meridional advection term is positive in SEA for both F09 and F05, which is different from the SEP region. This is probably related to the more complicated ocean current system in SEA, where southward Angola current and equatorward Benguela current meet. Previous study contributes the overshooting of warm Angola current to the SST warm bias (Xu et al. 2014), which is in agreement with the positive value of meridional advection in SEA region. Nevertheless, horizontal advection plays a less important role in upwelling area for both F09 and F05. The residual error caused by unresolved high-frequency

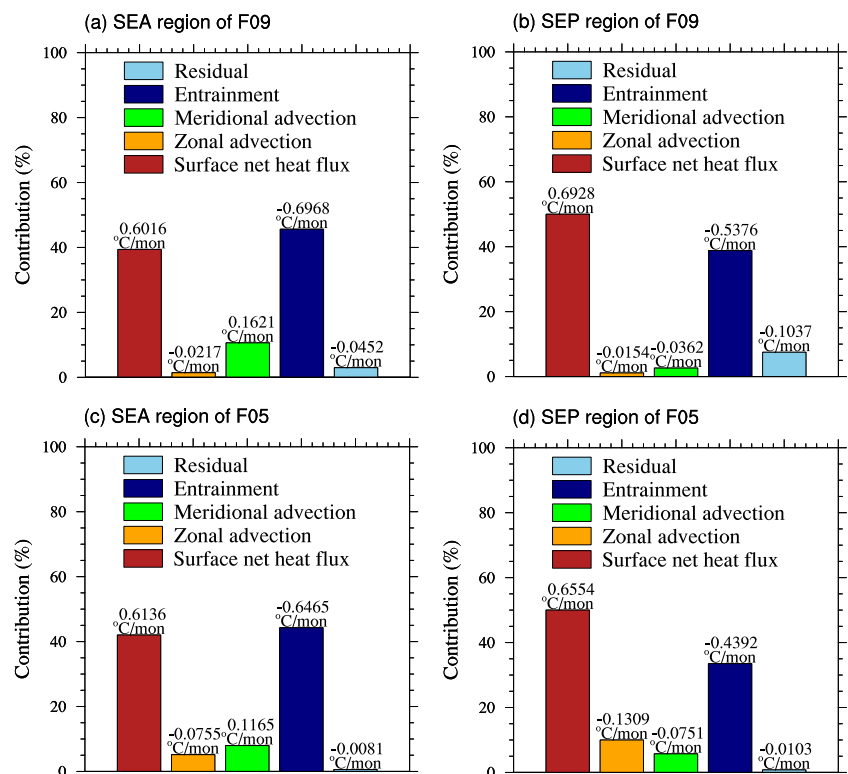
variability, diffusion term, and so on is small, and therefore ignored from analysis. As a result, we focus on the net surface heat flux and upwelling process of CESM in the following analysis of SST warm bias.

### 3.2 Underestimation of stratocumulus cloud

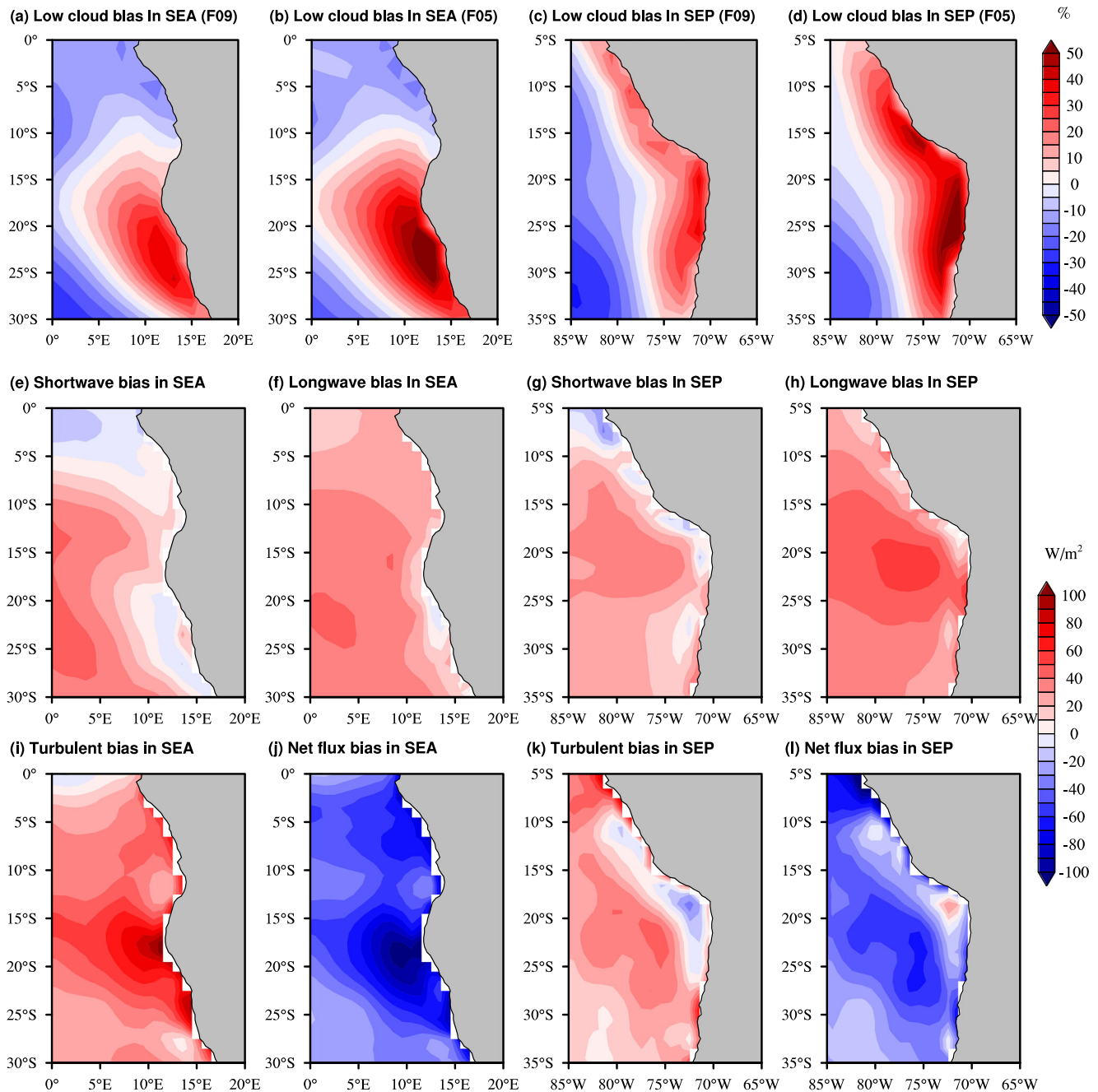
Underestimation of stratocumulus cloud has been regarded as one of the main reasons for SST warm biases: less stratocumulus cloud fraction enables more shortwave radiation reaching sea surface and hence the positive feedback. Figure 3a–d show CESM stratocumulus cloud bias in SEA and SEP, relative to CloudSat climatology in F05 and F09 experiment, respectively. On the open ocean, far away from the coast, the stratocumulus cloud is indeed underestimated by CESM. Correspondingly, ocean surface net short-wave radiation is larger than OAFflux values off Benguela and Peru-Chile coast, respectively (Fig. 3e, g). However, the modeled stratocumulus cloud fraction is higher than satellite data near the coast, which is not consistent with previous studies, indicating stratocumulus bias is not the primary reason for warm bias alongshore. Furthermore, the experiment with finer atmospheric resolution (F05) shows larger CESM low cloud bias, which means the improvement of SST simulation in F05 is due to other factors.

Figure 3e–l show surface heat flux bias over OAFflux climatology: subfigures e and g represent net shortwave radiation reaching ocean surface (positive downward);

**Fig. 2** SEA and SEP (blue rectangle regions in Fig. 1) area averaged contributions of each term in Eq. 1 for (a) (b): F09 experiment. (c) (d): F05 experiment







**Fig. 3** Stratocumulus cloud fraction bias modeled by CESM in SEA and SEP regions (top panel), relative to CloudSat climatology derived from July 2006 to December 2010: (a)(c) F09 experiment, (b)(d) F05 experiment. Flux biases of F09 in SEA and SEP, with respect to

OAFflux 1984–2009 mean: (e)(g) net shortwave, (f)(h) net longwave, (i)(k) sensible and latent heat flux, and (j)(l) net surface flux. Shortwave and net surface flux is positive downward, while longwave and turbulent (sensible plus latent heat) is positive upward

subfigures f and h represent net longwave radiation (positive upward); subfigures i and k represent sensible flux plus latent flux (positive upward); subfigures j and l are ocean surface net heat flux (positive downward, i.e.,  $j=e-f-i$ ). Less net shortwave radiation (with respect to OAFflux), in part, reaches ocean surface near Benguela and Peru-Chile

coast (Fig. 3e, g), which corresponds to nearshore larger stratocumulus cloud bias shown in Fig. 3a and c. On the open ocean, off from the Benguela and Peru-Chile coast, excessive shortwave radiation is overcompensated by upward longwave radiation (Fig. 3f, h), latent flux, and sensible flux (Fig. 3i, k). As a result, the surface net flux

is much lower compared with OAFlex on the open ocean (Fig. 3j, l). In this case, the simulated SST should be cooler, indicating warm bias probably is due to insufficient coastal upwelling. SEP has positive net surface flux bias near shore, coinciding with downward shortwave radiation bias and turbulent bias. While in SEA, upward turbulent bias is dominant, resulting in negative net surface flux bias. Thereinto, latent flux exerts considerable influence in accordance with larger SST warm bias in SEA. In short, SST warm bias alongshore is not predominantly due to surface net heat flux bias but ocean upwelling process.

### 3.3 Surface low-level coastal wind

Alongshore currents and upwelling process are extremely sensitive to the intensity and structure of nearshore surface wind. However, CESM of low-resolution atmospheric component has relatively poor representation of coastal wind simulation. Figure 4 shows wind stress from CFSR, F09, and F05 in SEA and SEP regions. It is evident that the structure of coastal wind stress demonstrates two maximum cores in SEA region from CFSR, located at near 17.5°S and 28°S latitude (Fig. 4a), respectively. In Patricola's article (2017), similar analysis is carried out. While in both F09 and F05 cases, this structure is poorly represented. Alongshore wind structure in SEP shows similar character, two extrema are situated in approximate 15°S and 30°S, in accordance with previous result (Colas et al. 2012). Besides, wind stress maximum is displaced far from Benguela and Peru-Chile coast in both F09 and F05. Furthermore, the northern extrema are much weaker. Finer resolution case F05 comparatively has better realistic representation of wind stress structure than F09, magnitude of extrema is larger and closer to coast, suggesting atmosphere horizontal resolution exerts a considerable influence on alongshore wind. This is consistent with existing works (Patricola and Chang 2017), in which various observational and modeling results with different resolutions are adopted, to conclude that the finer resolution enables more accurate low-level coastal jets. For this region, there exists wind pattern in the zonal direction across the land-sea boundary. First, the meridional wind strength gradually increases while approaching this boundary from the open ocean. Second, at the proximity of the boundary, the wind strength decreases abruptly and to a very low level on the land. With CFSR data, Fig. 5 shows the 10-m wind velocity-longitude cross-section at 17.5°S of SEA and 15°S of SEP where northern maximum is located, respectively. Through the comparison, we conclude that CFSR's representation of wind drop-off alongshore is relatively realistic, secondly F05, followed by F09, and COREv2 data the worst.

### 3.4 Ocean's responses

Ocean's dynamic and thermodynamic response to the atmospheric wind stress and curl is mainly determined by the following aspects. First, when coastal prevailing wind is in equatorward direction of EBUS regions, Ekman offshore currents ensue, leading to coastal upwelling here. Meanwhile, alongshore wind could generate downwind ocean coastal currents to some extent (Philander and Yoon 1982). Furthermore, negative wind stress curl is beneficial to Ekman pumping-driven upwelling in SEP and SEA (Pickett and Paduan 2003; Small et al. 2015). Last, excessive poleward warm water transport is driven by negative offshore wind stress curl in SEA, leading to warm SST bias (Small et al. 2015). According to Small et al. (2015), Sverdrup balance plays an important role in transporting equator warm water southward when the band of modeled negative wind stress curl is broad and far from coast.

As discussed in Section 3.3, modeled alongshore surface wind jet is very weak in CESM, preventing ocean's inner water from upwelling. F05 has improvement in simulating coastal surface wind, resulting in better representation of upper ocean process. Meanwhile, wind stress curl in F09 (Fig. 6a, c) is also broad and located farther from coast, resulting in Ekman pumping maximum lying offshore (Fig. 7a, c). In contrast, wind stress curl band of F05 is narrower and closer to coast (Fig. 6b, d), promoting currents upwelling nearshore (Fig. 7b, d). F05 has stronger upwelling responses nearshore, with more cold deep water reaching surface. In addition, horizontal transport also is found to have profound effect on surface temperature. Wind stress curl (Fig. 6) and vertical-integrated meridional mass transport (Fig. 7e–h) represent two sides of equal sign of Sverdrup balance: wind stress curl is balanced by vertical-integrated meridional mass transport. The patterns both indicate that negative wind stress curl in the Southern Hemisphere could generate poleward water transportation. As a result, the water from deep to top is driven southward near coast region, and surface meridional velocity is poleward in most nearshore region, not in the downwind direction. However, in F05, weaker poleward mass transport is present due to narrower wind stress curl. This is consistent that Sverdrup balance is applicable for large-scale, geostrophic flow (Small et al. 2015), but does not apply for this finer resolution situation.

Compared with SEP, in SEA region, cold northward Benguela Current and warm southward Angola Current converge near 16°S, forming Angola-Benguela front (ABF). SST warm bias in this region is attributed to the modeled southward shift of ABF. The latitude where ABF resides is usually characterized by large temperature gradient or

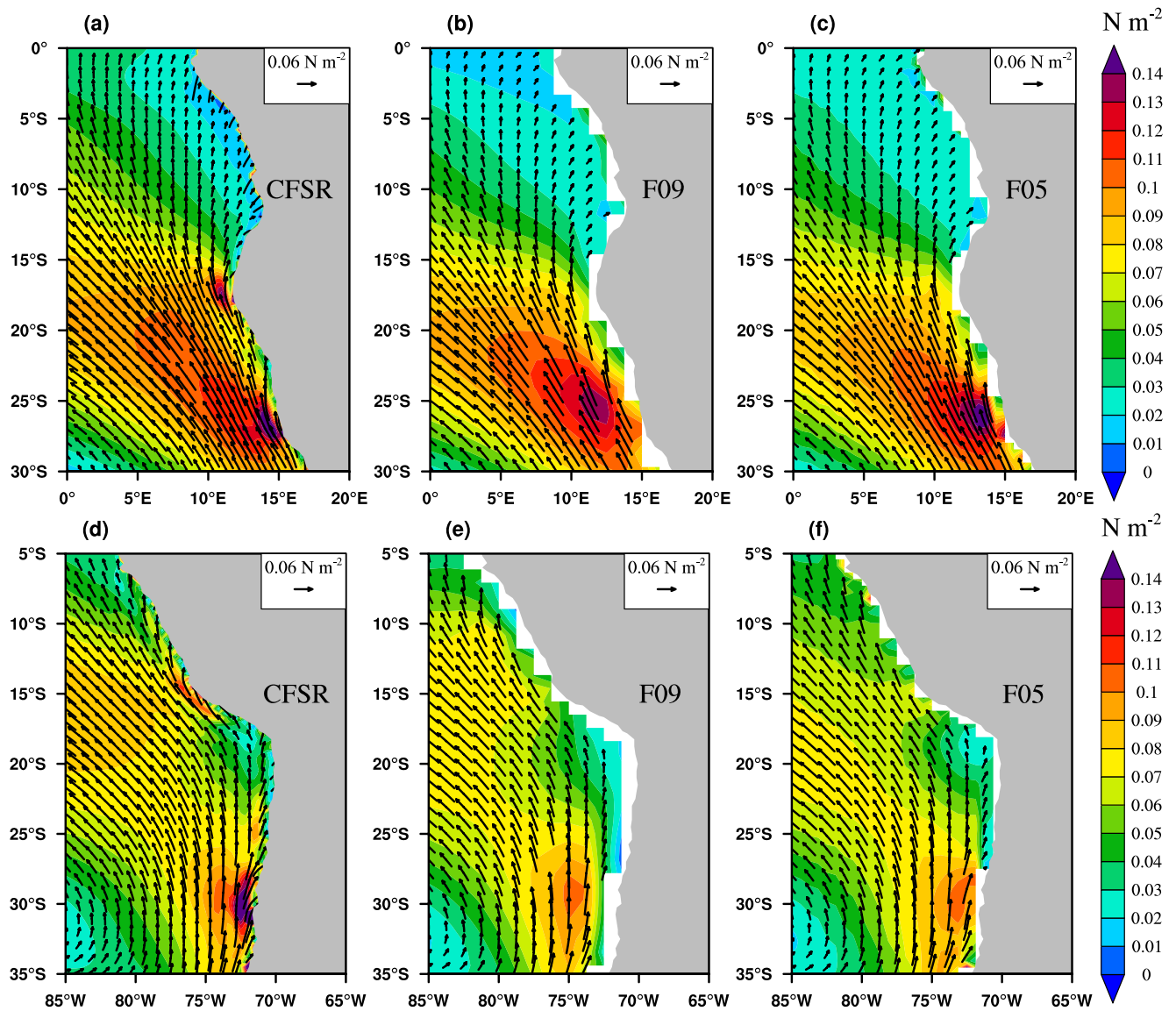
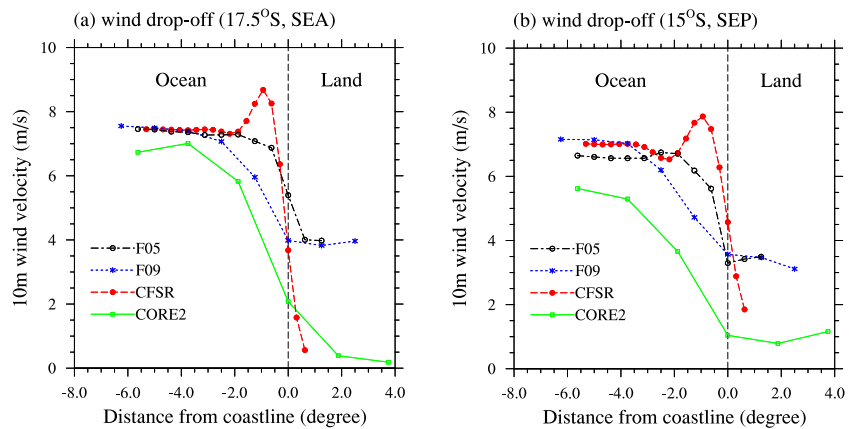
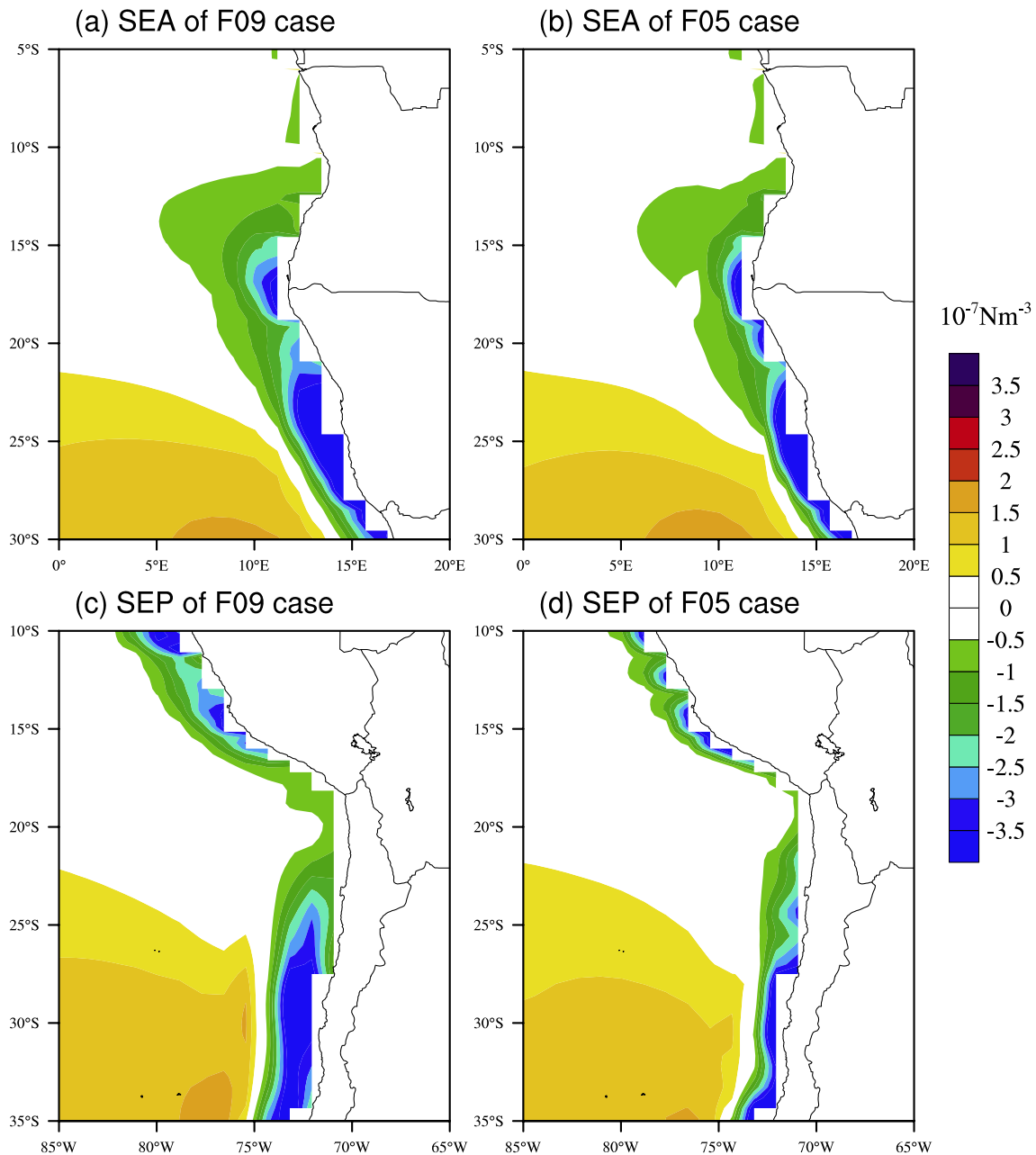


Fig. 4 Wind stress vector and magnitude of CFSR (a and d), F09 (b and e), and F05 (c and f). Top panels: SEA; bottom panels: SEP

Fig. 5 10 m wind velocity-longitude cross-section at 17.5°S of SEA region (a) and 15°S of SEP region (b)







**Fig. 6** Wind stress curl of F09 (a and c) and F05 (b and d). Top panels: SEA region; bottom panels: SEP region

zero velocity. Therefore, ABF position of F09 and F05 is computed according to the position where subsurface mean velocity equals 0 and the maximum meridional temperature gradient is present (Fig. 8). With different definitions, consistent result is attained, as follows. The ABF position has a seasonal cycle, and is northernmost in August and September, same as in (Xu et al. 2014). On average, ABF is located at  $\sim 19^\circ\text{S}$  for F09, and  $21^\circ \sim 24^\circ\text{S}$  of F05. The position of ABF in F05 is more realistic, which is related to accurate wind stress curl (see above).

## 4 Sensitivity analysis with model topography

### 4.1 Comparison of topography

Coastal low-level wind is related to the land-sea temperature gradient and coastal high land topography. Peru-Chile and Namibia regions feature significant coastal topographies, which are major contributions to alongshore wind generation. Some studies suggest that failure of resolving the orography is responsible for weak alongshore wind

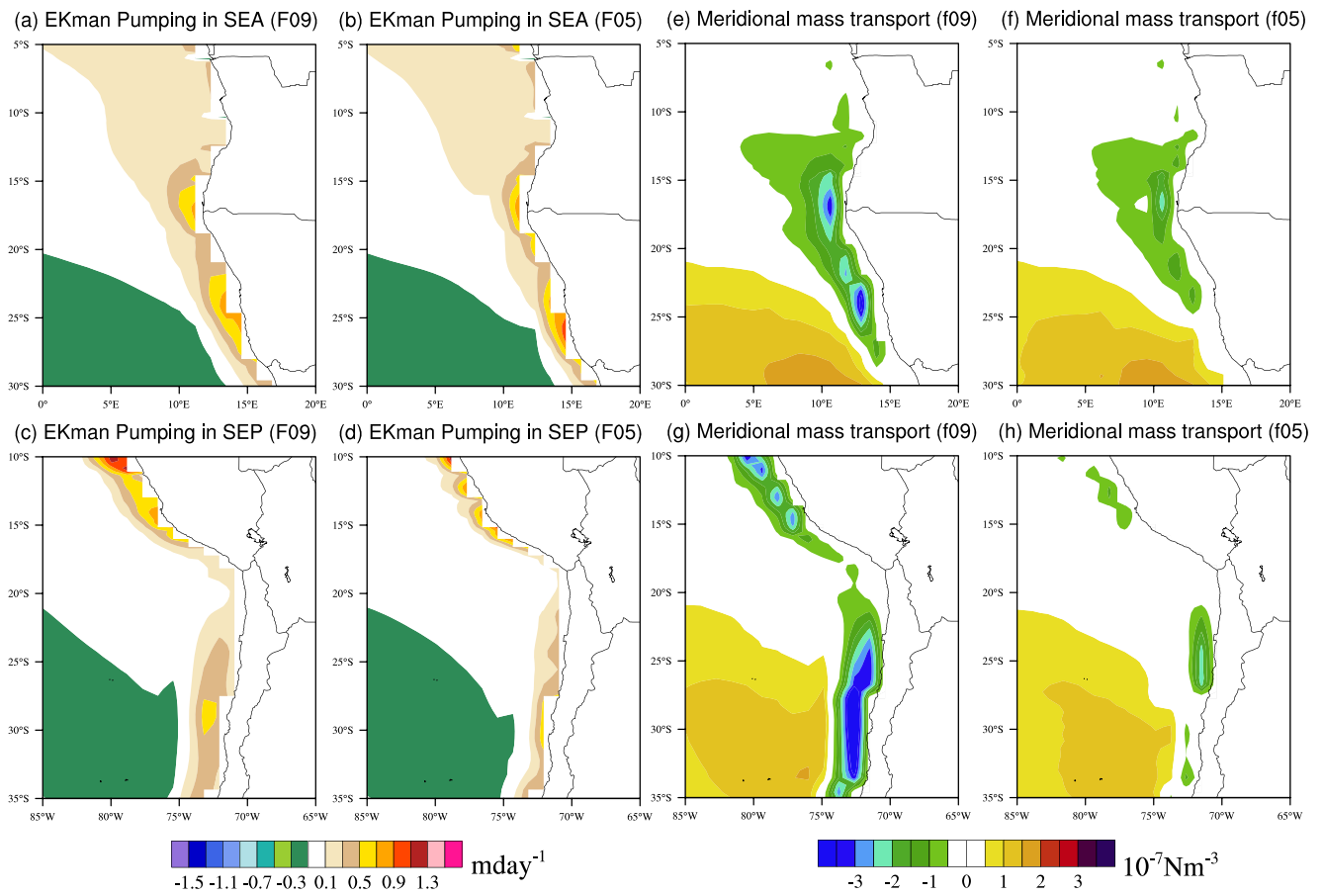


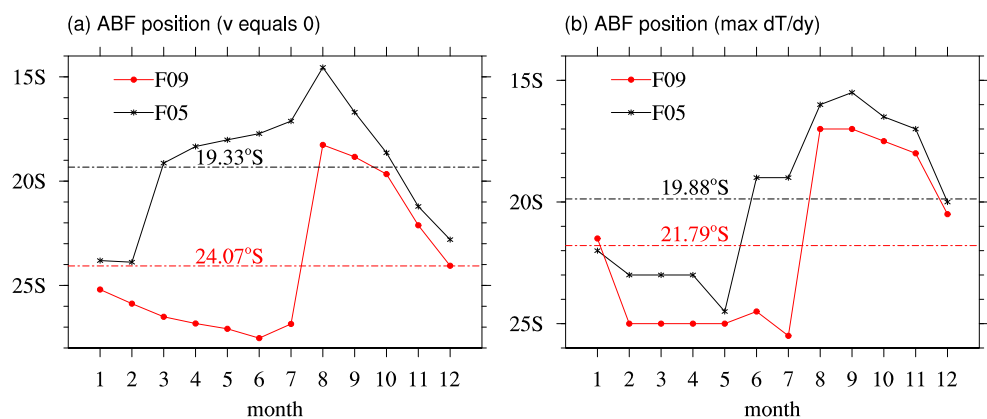
**Fig. 7** Ekman pumping of F09 (a), (c) and F05 (b), (d); Meridional oceanic mass transport (vertically integrated) of F09 (e), (g) and F05 (f), (h). Top panels: SEA region; right panels: SEP region

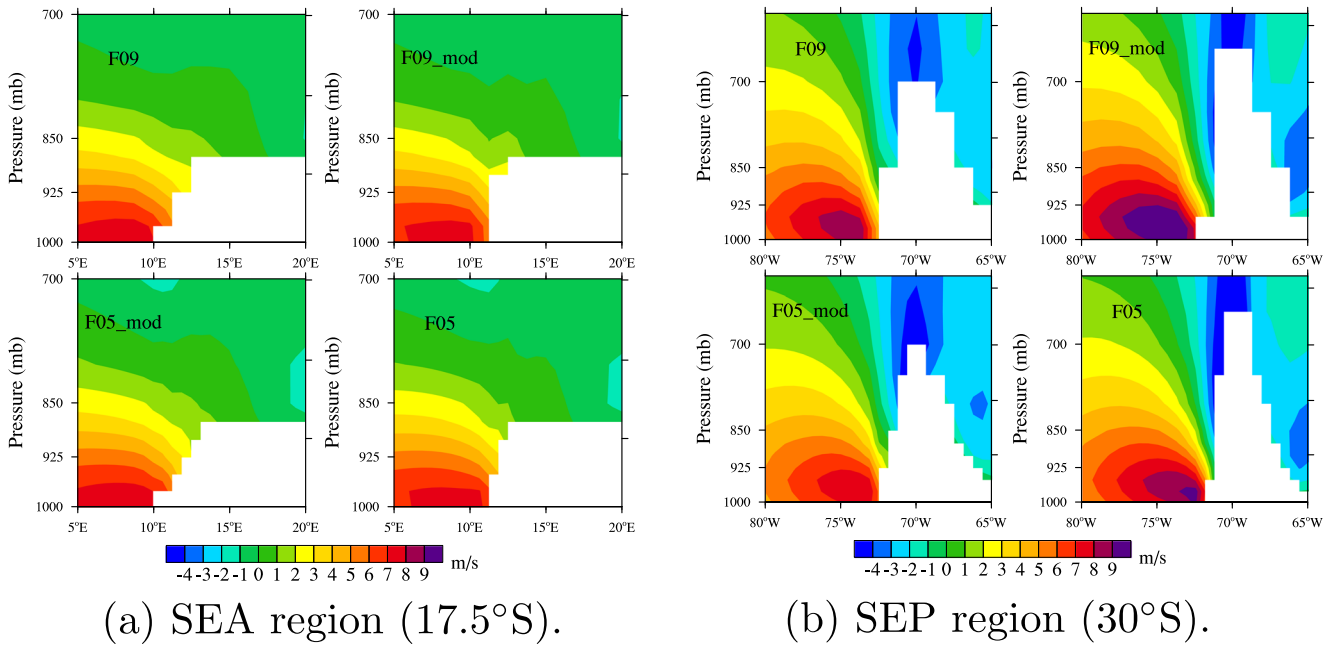
(Colas et al. 2012; Large and Danabasoglu 2006). This study carried out 2 comparative experiments to further explore whether better resolved land topography can lead to better representation of wind structure with finer atmospheric resolution (F05). F09\_mod (F05\_mod) is run as same as F09 (F05) except that the Africa and South America land topography is replaced by F05 (F09), as shown in Table 1.

Figure 9 shows the meridional wind vertical cross-section at 17.5°S of SEA and 30°S of SEP. The white patch in each

figure represents land topography. Among four experiments, F05 has the steepest topography, and F05\_mod becomes much smoother than F05 after topography replacement. Similarly, topography of F09 is smooth, and F09\_mod is much steeper. As a result, the meridional wind becomes much more stronger close to steeper slope (e.g., F05 and F09\_mod), especially in SEP due to steeper and more realistic topography than SEA. In SEA, the alongshore topography is not as high as that in SEP region and topography replacement causes little

**Fig. 8** ABF position of F09 and F05, calculated according to: **a** subsurface mean velocity equals 0 and **b** maximum meridional temperature gradient





**Fig. 9** Vertical cross-section of meridional wind at  $17.5^{\circ}\text{S}$  of SEA region (a) and  $30^{\circ}\text{S}$  of SEP region (b)

change, with the wind structure almost the same (F05\_mod versus F05, and F09\_mod versus F09).

As a result, the differences of the modeled SST differences are shown in Fig. 10. After topography replacement, SST of F09\_mod (F05\_mod) is much cooler (warmer)

than F09 (F05), and much warmer (cooler) than F05 (F09) in SEP. This is consistent with the alongshore wind stress strength due to the topography steepness. As a contrary, in SEA, SST shows little change as model topography in F05 and F09 is not significant.

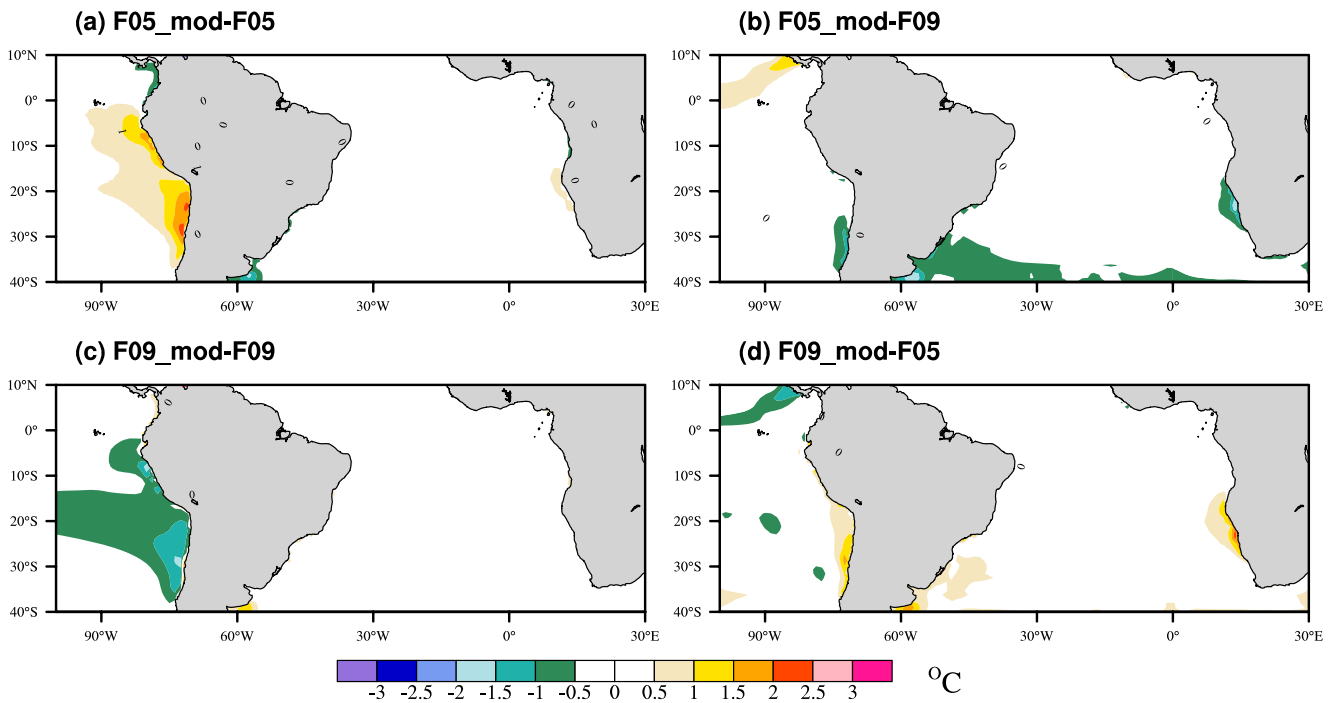


**Fig. 10** SST difference of four experiments

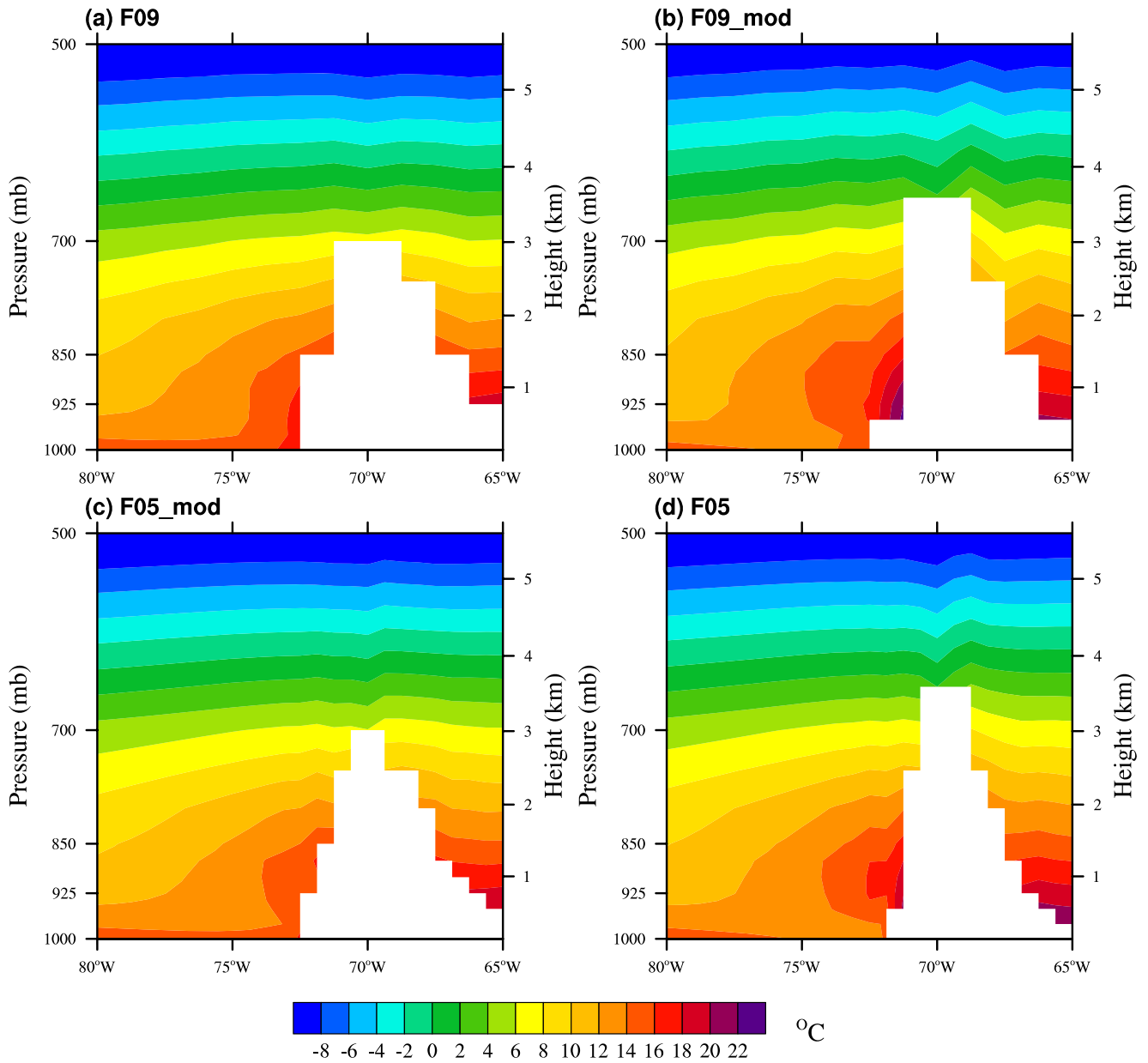
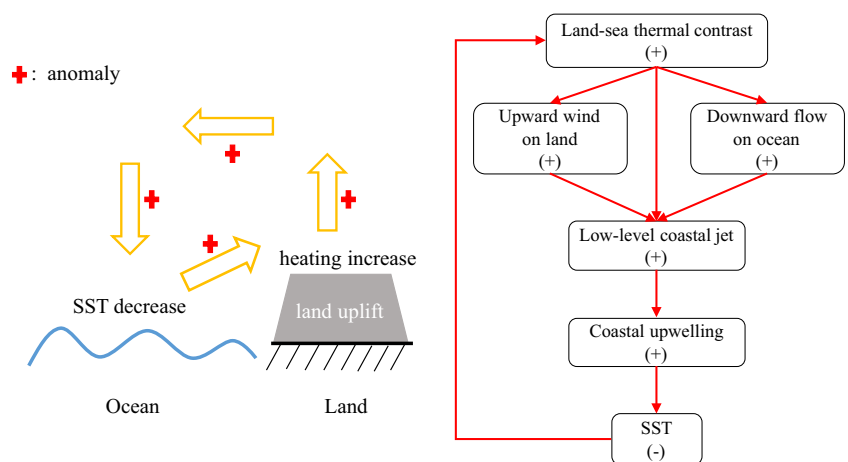


**Fig. 11** Air temperature vertical cross-section at 30°S in SEP of four experiments

**Fig. 12** The positive feedback mechanism of land-sea temperature gradient's effect on SST



### 4.2 Sensitivity analysis of topography

To explore the potential physical mechanism, we further study the impact of topography. Figure 11 shows the vertical cross-section of air temperature at 30°S in all 4 experiments. In higher and steeper topography experiments (F09\_mod and F05), land heating anomalies is present above land surface and cooler temperature anomalies on sea surface, which is in direct contrast with F09 and F05\_mod, respectively. Both contribute to larger land-sea temperature gradient, which enables further intensification of alongshore low-level wind. Here, we use positive feedback mechanism shown in Fig. 12 to explain the whole process. The increased

upward anomalous wind on land due to extra land heating and the accompanying anomalous downward flow on the ocean due to cooler sea surface temperature anomalies together promote the amplification of air circulation. As a result, under the effect of thermal wind and significant mountain topography blocking, alongshore low-level coastal jet is also strengthened (Fig. 13a, b). As a combined result, ocean coastal upwelling is intensified, resulting in cooler sea surface temperature (Fig. 10a, c). In return, cooler SST increases land-sea thermal contrast, which forms the positive feedback mechanism.

Evidences of positive feedback are also provided in Fig. 13c–f. F09\_mod displays considerably more strato-

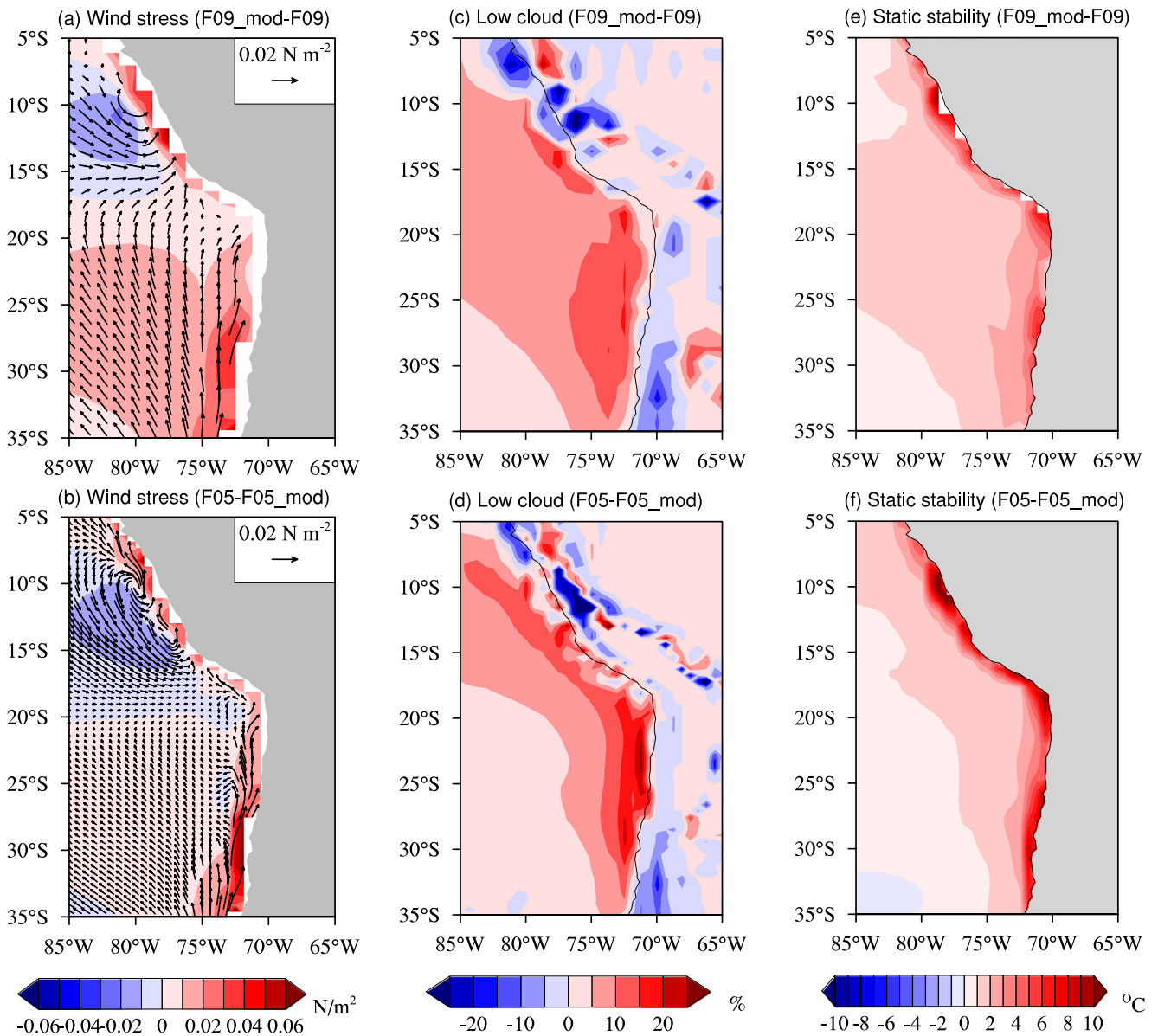


**Fig. 13** The difference between F09\_mod (F05) and F09 (F05\_mod) of wind stress (a), (b), stratocumulus cloud (c), (d), and atmosphere static stability (e), (f)



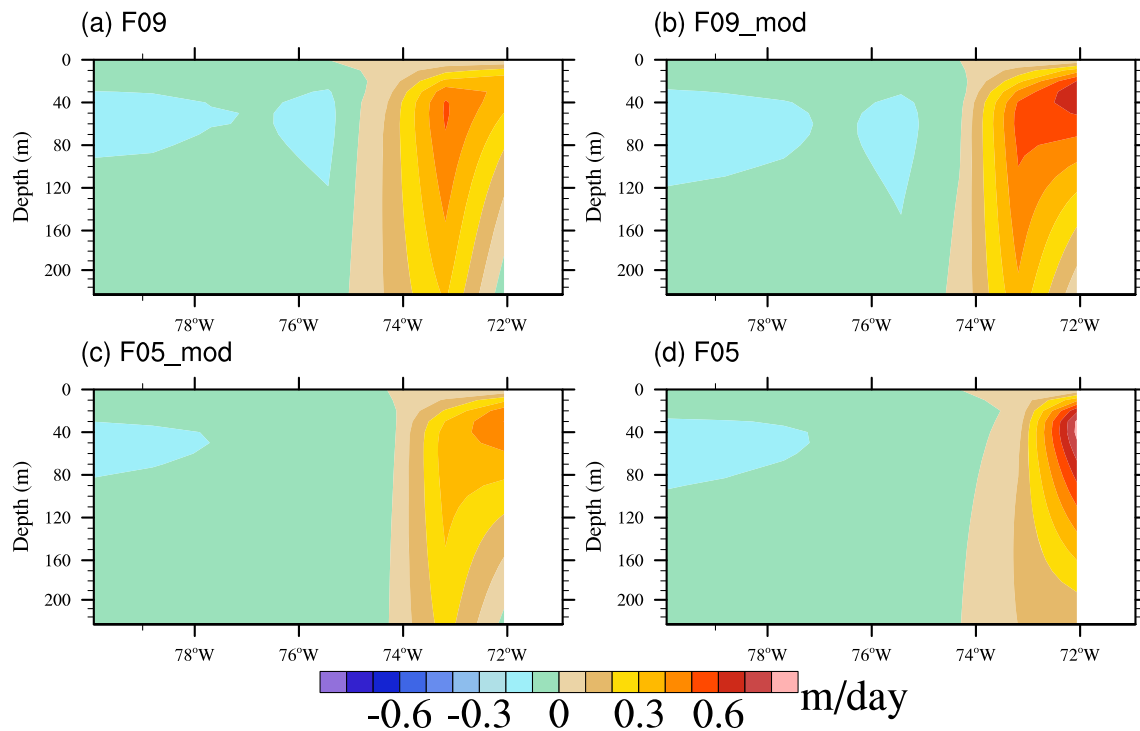


**Fig. 14** Subsurface ocean vertical velocity in 30° of SEP

cumulus cloud owing to downward flow anomalies in coastal ocean side than F09, and less in coastal land side due to upward wind anomalies (Fig. 13c).

Given that the static stability of the atmosphere over coastal ocean can affect the formation of stratocumulus clouds, we next evaluate stability by measuring the difference between surface and 700 *hPa* potential temperature. The difference of static stability between F09\_mod and F09 is shown in Fig. 13e. F09\_mod shows more stable atmosphere stratification, which is favorable for the formation of low clouds. Comparison between F05 and F05\_mod show similar results in Fig. 13f.

The influence of low-level coastal jet amplification on ocean dynamical process is already discussed in Section 3.4. Strengthened coastal low-level wind and its curl results in stronger Ekman pumping–driven upwelling and meridional transport of relatively cold water, leading to the cooling of SST. In this cases, the maximum of subsurface ocean vertical velocity is stronger and closer to land in F09\_mod (F05) than F09 (F05\_mod) (Fig. 14). For the horizontal perspective, vertically integrated equatorial water transport is stronger in F09\_mod than F09 (not shown). In all, higher land topography benefits strengthened low-level coastal jet, resulting in cooler sea surface temperature. The result indicates that more accurate SST simulation of finer atmosphere resolution model (e.g., F05) in SEP region is mainly caused by better resolved significant topography.

## 5 Summary and conclusion

This article aims to explore the causes of sea surface temperature warm bias in EBUS regions in climate models such as CESM, by focusing on Southeast Pacific and Southeast Atlantic. Through the breakdown of the energy budget of upper ocean, we conclude surface net heat flux and Ekman upwelling process together contribute over 80% to SST bias in EBUS for CESM. Although underestimation of stratocumulus cloud has been regarded as one of major sources of warm bias in open ocean, we show reliable evidence that this is not the key cause for alongshore regions, where most severe SST warm bias resides. On the contrary, low cloud fraction is overestimated near coast, leading to excessive solar radiation reaching ocean surface. Finer atmosphere grid resolution results in even more low cloud alongshore, which contradicts with the lower SST bias. Secondly, net surface energy flux suggests that cooling bias due to excessive shortwave radiation is overcompensated by longwave radiation and latent flux biases. Therefore, the insufficient ocean upwelling process plays a more important role in SST warm bias, with wind stress and its curl dominating the dynamics of the upwelling system and the thermodynamic responses. Stronger and closer wind stress and curl could lead to realistic representation of upwelling and cold water advection. Through comparison of different atmosphere resolution model simulations, we conclude that finer atmosphere horizontal

resolution is required for coupled models to simulate the accurate low-level coastal jet and the upwelling system. When coastal wind is well represented, the vertical upwelling is much stronger and poleward horizontal transportation as estimated by Sverdrup balance is not applicable. Meanwhile, the ABF position is no more southerly displaced without the southward intrusion of Angola Current. Further simulations with modified model topography shows that the abrupt high topography in SEP significantly affects alongshore wind and SST, by increasing land-sea temperature contrast and the positive feedback mechanism. With relatively lower resolution, more realistic model topography enables better representation of wind structure. Combined with higher resolution, smaller SST bias can be achieved with coupled models for both EBUS regions.

When contrasting southeast Pacific and southeast Atlantic, different processes dominate. In terms of physical geography, Namibia features no significant topography as high as Peru-Chile. As a result, finer resolution atmosphere model plays a more important role in improving the accuracy of SST simulation in SEP. On the other side, ocean currents of SEP are not as complicated as SEA, for which Benguela Current and Angola Current creates ABF and much harder to simulate with low-resolution models. Although there exists practical limitations of model resolution in climate studies, adopting higher resolutions is necessary for the simulation of realistic upwelling systems. Beyond the modeling the physical climate, it is also essential to accurately project biogeochemical processes and changes, given the importance of EBUS regions in this aspect. Model improvements, such as variable resolution approaches, can be adopted for accurate and practical simulation of EBUS regions, which serve as future studies.

**Acknowledgements** The authors thank the editor and referees for their invaluable efforts in improving the manuscript.

**Funding information** This work is partially supported by the National Key R & D Program of China under the grant number 2017YFA0603902 and the General Program of National Science Foundation of China under the grant number 41575076. This work is also partially supported by Center for High-Performance Computing and System Simulation, Pilot National Laboratory for Marine Science and Technology (Qingdao).

## References

- Breugem WP, Chang P, Jang CJ, Mignot J, Hazeleger W (2010) Barrier layers and tropical Atlantic SST biases in coupled GCMs. *Tellus Series A-dynamic Meteorology And Oceanography* 60(5):885–897
- Colas F, McWilliams JC, Capet X, Kurian J (2012) Heat balance and eddies in the Peru-Chile current system. *Clim Dyn* 39(1-2):509–529
- Danabasoglu G, Bates SC, Briegleb BP, Jayne SR, Jochum M, Large WG, Peacock S, Yeager SG (2012) The CCSM4 ocean component. *J Clim* 25(5):1361–1389
- Gent PR, Yeager SG, Neale RB, Levis S, Bailey DA (2010) Improvements in a half degree atmosphere/land version of the CCSM. *Clim Dyn* 34(6):819–833
- Holt TR (1996) Mesoscale forcing of a boundary layer jet along the California coast. *J Geophys Res-Atmos* 101(D2):4235–4254
- Hu ZZ, Huang B, Pegion K (2008) Low cloud errors over the southeastern Atlantic in the NCEP CFS and their association with lower-tropospheric stability and air-sea interaction. *J Geophys Res-Atmos* 113(D12)
- Huang B, Hu ZZ, Jha B (2007) Evolution of model systematic errors in the tropical Atlantic basin from coupled climate hindcasts. *Clim Dyn* 28(7-8):661–682
- Hunke EC, Lipscomb WH (2008) CICE: the Los Alamos sea ice model documentation and software user's manual version 4.0 la-cc-06-012. In: Version 4.0, LA-CC-06-012, Los Alamos National Laboratory
- Hurrell JW, Holland MM, Gent PR, Ghan S, Kay JE, Kushner PJ, Lamarque JF, Large WG, Lawrence D, Lindsay K (2013) The community earth system model: a framework for collaborative research. *Bull Am Meteorol Soc* 94(9):1339–1360
- Hurrell JW, Hack JJ, Shea D et al (2008) A new sea surface temperature and sea ice boundary dataset for the community atmosphere model. *J Clim* 21(19):5145–5153
- Jung G, Prange M, Schulz M (2014) Uplift of Africa as a potential cause for Neogene intensification of the Benguela upwelling system. *Nat Geosci* 7(10):741–747
- Large WG, Danabasoglu G (2006) Attribution and impacts of upper-ocean biases in CCSM3. *J Clim* 19(11):2325–2346
- Large WG, Yeager SG (2009) The global climatology of an inter-annually varying air-sea flux data set. *Clim Dyn* 33(2-3):341–364
- Ma CC, Mechoso CR, Robertson AW, Arakawa A (1996) Peruvian stratus clouds and the tropical Pacific circulation: a coupled ocean-atmosphere GCM study. *J Clim* 9(7):1635–1645
- Menkes CER, Vialard JG, Kennan SC, Boulanger JP, Madec GV (2006) A modeling study of the impact of tropical instability waves on the heat budget of the eastern equatorial Pacific. *J Phys Oceanogr* 36(36):847–865
- Mohrholz V, Schmidt M, Lutjeharms JRE (2001) The hydrography and dynamics of the Angola-Benguela frontal zone and environment in April 1999. *S Afr J Sci* 97(5):199–208
- Neale RB, Richter J, Park S, Lauritzen PH, Vavrus SJ, Rasch PJ, Zhang M (2013) The mean climate of the community atmosphere model (CAM4) in forced SST and fully coupled experiments. *J Clim* 26(14):5150–5168
- Oleson KW, Niu GY, Yang ZA, Lawrence DM, Thornton PE, Lawrence PJ, Stackli R, Dickinson RE, Bonan GB, Levis S (2015) Improvements to the community land model and their impact on the hydrological cycle. *J Geophys Res Biogeosci* 113(G1):G01,021
- Patricola CM, Chang P (2017) Structure and dynamics of the Benguela low-level coastal jet. *Clim Dyn* 49(7-8):1–24
- Patricola CM, Li M, Xu Z, Chang P, Saravanan R, Hsieh JS (2012) An investigation of tropical Atlantic bias in a high-resolution coupled regional climate model. *Clim Dyn* 39(9-10):2443–2463
- Philander SGH, Yoon JH (1982) Eastern boundary currents and coastal upwelling. *J Phys Oceanogr* 12(12):862–879
- Pickett MH, Paduan JD (2003) Ekman transport and pumping in the California current based on the U.S. navy's high-resolution atmospheric model (COAMPS) *J Geophys Res Oceans*. 108(C10)
- Richter I (2015) Climate model biases in the eastern tropical oceans: causes, impacts and ways forward. *Wiley Interdiscip Rev Clim Change* 6(3):345–358

- Richter I, Xie SP, Wittenberg AT, Masumoto Y (2011) Tropical Atlantic biases and their relation to surface wind stress and terrestrial precipitation. *Clim Dyn* 38(5):985–1001
- Saha S, Moorthi S, Wu X, Wang J, Nadiga S, Tripp P, Behringer D, Hou YT, Chuang HY, Iredell M (2012) The NCEP climate forecast system version 2. *J Clim* 27(6):2185–2208
- Shannon LV, Agenbag JJ, Buys MEL (1987) Large- and mesoscale features of the Angola-Benguela front. *S Afr J Mar Sci* 5(1):11–34
- Small RJ, Curchitser E, Hedstrom K, Kauffman B, Large WG (2015) The Benguela upwelling system: quantifying the sensitivity to resolution and coastal wind representation in a global climate model. *J Clim* 28(23):150921125611,001
- Stephens GL, Vane DG, Boain RJ, Mace GG, Sassen K, Wang Z, Illingworth AJ, O’connor EJ, Rossow WB, Durden SL, Miller SD (2002) The CloudSat mission and the A-Train: a new dimension of space-based observations of clouds and precipitation. *Bull Am Meteorol Soc* 83(12):1771–1790
- Taylor KE, Stouffer RJ, Meehl GA (2012) An overview of CMIP5 and the experiment design. *Bull Am Meteorol Soc* 93(4):485–498
- Wahl S, Latif M, Park W, Keenlyside N (2011) On the tropical Atlantic SST warm bias in the Kiel climate model. *Clim Dyn* 36(5-6):891–906
- Wang C, Zhang L, Lee SK, Wu L, Mechoso CR (2014) A global perspective on CMIP5 climate model biases. *Nat Clim Chang* (3):201–205
- Xu Z, Chang P, Richter I, Kim W, Tang G (2014) Diagnosing southeast tropical Atlantic SST and ocean circulation biases in the CMIP5 ensemble. *Clim Dyn* 43(11):3123–3145
- Xu Z, Li M, Patricola CM, Chang P (2014) Oceanic origin of southeast tropical Atlantic biases. *Clim Dyn* 43(11):2915–2930
- Yu L, Haines K, Bourassa M, Cronin M, Gulev S, Josey S, Kato S, Kumar A, Lee T, Roemmich D (2012) Towards achieving global closure of ocean heat and freshwater budgets: recommendations for advancing research in air-sea fluxes through collaborative activities
- Zheng Y, Shinoda T, Kiladis GN, Lin J, Metzger EJ, Hurlburt HE, Giese BS (2012) Upper ocean processes under the stratus cloud deck in the southeast Pacific Ocean. *J Phys Oceanogr* 40(1):103–120